Article

Impact of Ship Emissions on Air Quality in the Guangdong-Hong Kong-Macao Greater Bay Area (GBA): With a Particular Focus on the Role of Onshore Wind

Qinyu Cheng, Xiaotong Wang, Dongsheng Chen *, Yizhe Ma, Ying Zhao, Jianghong Hao, Xiurui Guo, Jianlei Lang and Ying Zhou

Key Laboratory of Beijing on Regional Air Pollution Control, Beijing University of Technology, Beijing 100124, China; cheng0527777@emails.bjut.edu.cn (Q.C.); wangxt@bjut.edu.cn (X.W.); mayizhe1164@emails.bjut.edu.cn (Y.M.); yzhao@emails.bjut.edu.cn (Y.Z.); haojianghong@emails.bjut.edu.cn (J.H.); guoxiurui@bjut.edu.cn (X.G.); jllang@bjut.edu.cn (J.L.); y.zhou@bjut.edu.cn (Y.Z.)
* Correspondence: dschen@bjut.edu.cn; Tel.: +86-10-6739-1659

Abstract: Background: ship emissions have an adverse effect on air quality in coastal regions, and this effect can be exacerbated by onshore winds. Objectives and methods: to investigate the impact of ship emissions on air pollutant concentrations during the onshore wind period in a low-latitude region in China, this study applied the WRF/Chem model to simulate the contribution of ship emissions to $PM_{2.5}$ and O_3 by "zero-out" in 2018, in the Guangdong-Hong Kong-Macao Greater Bay Area (GBA). Results/findings: results show that the onshore winds facilitated the transport of ship-emitted pollutants to inland areas, causing the contribution of ship emissions to $PM_{2.5}$ exceeding 4 µg/m^3 to areas north of Guangzhou in April and west of the GBA in October. The impact of onshore winds on the ship contribution to the O_3 concentration shows a bidirectional trend both spatially and monthly. The onshore winds raised the ship contribution to O_3 concentrations in April by 1.54 µg/m^3, while exacerbated the decreasing contribution in other months. In VOC-sensitive cities such as Foshan, onshore winds exacerbated the negative contribution of ship emissions to O_3 concentrations; while in NOx-sensitive cities such as Huizhou, they enhanced the contribution of ship-induced O_3. Novelty/Improvement: this paper fills a gap in the study of pollutants transportation characteristics from ship emissions under the influence of onshore winds in the GBA. Our results demonstrate the importance of considering meteorological conditions and atmospheric chemical mechanisms regarding the coastal air pollution prevention caused by ship emissions.

Keywords: ship emissions; onshore wind; GBA; $PM_{2.5}$; WRF/Chem

1. Introduction

The shipping industry is the lifeblood of the global economy, and it is responsible for more than 85% of the world's cargo transportation. As a major shipping country, China relies heavily on maritime transportation for its economic and social development. By the end of 2020, China's ports and the navigable mileage of inland waterways ranked first in the world [1]. With the continuous improvement of the waterway network and the increasing progress of navigation technology, China's ports are expected to handle more than 25 billion tons of cargo by 2030 [2]. As an important means of transportation for maritime logistics, ships, while undertaking busy passenger and cargo transportation, ships also cause a large number amount of air pollutants, including nitrogen oxide (NO$_x$), sulfur dioxide (SO$_2$), particulate matter (PM), and hydrocarbon (HC), etc. [3–5]. The transportation, diffusion and secondary transformation of ship-emitted pollutants lead to serious air pollution in coastal areas and even some inland areas [6–11], and then causes adverse effects on human health [9,12,13]. In order to alleviate air pollution caused by ships and promote the sustainable development of the maritime industry, it's necessary to

comprehensively understand the transportation characteristics of ship emissions and their impact on air quality.

The Guangdong-Hong Kong-Macau Greater Bay Area (GBA), located on the southeast coast of China, is one of the busiest shipping areas in the world. Distributed with dense shipping lanes and numerous ports, as well as the deep-into-inland Pearl River water system, the GBA region is undoubtedly largely affected by ship pollutants. Studies have shown that in 2015, ship emissions near the GBA region contributed 1.6 $\mu g/m^3$ to the annual concentration of $PM_{2.5}$ [10], and 1.9 $\mu g/m^3$ to the monthly concentration of O_3 in July [14]; Tao et al. [15] conducted a field observation study at two stations in Guangzhou and Zhuhai and found that ship emissions were the main source of $PM_{2.5}$, with a contribution of over 17%. As one of the most densely populated urban agglomerations in China, the high levels of exposure to ship pollutants would raise the health risk for many diseases, including respiratory diseases [16] and cardiovascular diseases [13]. It has been estimated that in 2015, hundreds of premature deaths could be attributed to air pollution caused by ship emissions in this region [14].

The dispersion of air pollutants in coastal regions could be affected by a combination of multiple factors, such as the topographic and meteorological conditions [17–20]. Among them, winds, as an important meteorological factor in coastal areas [21–24], can significantly affect the dispersion and transportation of pollutants emitted from ships. Onshore winds can drive pollutants to be transported inland, whereas offshore winds can transport pollutants to the sea [22,25]. Lv et al. [10] found that during the onshore wind period, ship emissions caused an average increase of 4.7–17.1% in $PM_{2.5}$ concentrations in some cities in the Yangtze River Delta (YRD) of Eastern China, which was about 1.8–2.7 times higher than other days. Liu et al. [26] found that in the background of onshore wind, the contribution of ship emissions to $PM_{2.5}$ concentrations in the coastal area of Shanghai could reach 3–7 $\mu g/m^3$, accounting for 15–20% of the total $PM_{2.5}$ concentration. Our previous studies [27,28] preliminarily explored the effect of ship emissions on $PM_{2.5}$ in the Bohai Rim region under the background of sea breeze, and found that ship emissions contribute 1.3 $\mu g/m^3$ more to $PM_{2.5}$ concentrations during the onshore wind period compared to that during non-onshore wind periods.

Although these studies have investigated the impact of onshore winds on the transportation of ship emissions, but most of them were targeted at mid-latitude areas (e.g., Bohai Rim and Yangtze River Delta) and the research focused on low latitude areas has not yet been found. The winding coastline and more complex wind conditions on the north coast of the South China Sea exacerbate the complexity of air pollution formation [17,29,30], and its impact on the ship-induced air pollution in the GBA region deserves further investigation. Moreover, most of the air pollutants of interest in current studies were $PM_{2.5}$ in terms of ship-induced air pollution, and less attention was paid to O_3. Considering the demand for collaborative emission reduction of multiple pollutants, the effect of ship emissions on O_3 concentration also needs to be quantified.

To fill these gaps, our study aims to provide a comprehensive investigation of the impact of ship emission on air quality in the GBA, in which the effect of onshore winds on the transportation and transformation of ship-emitted pollutants will be quantified. The specific research objectives are as follows:

(1) Comprehensively quantifying the impact of ship emissions on air quality in the GBA region in different month in 2018, including the atmospheric concentration of NO_2, $PM_{2.5}$ and O_3.

(2) Enabling a better understanding of the local onshore wind feature by establishing onshore wind datasets for the four representative months of January, April, July, and October in 2018 for the GBA region.

(3) Characterizing the spatial and temporal influence of onshore winds in the transportation characteristics of air pollutant emissions from ships in a typical low-latitude coastal urban area.

To achieve the above objectives, the Weather Research and Forecast model combined with the Chemistry (WRF/Chem) modelling system was employed to simulate the impact of ship emissions on the air quality in the GBA in four months (January, April, July and October) in 2018. The spatial distribution and monthly variation of the contribution of ship emissions to the atmospheric NO_2, $PM_{2.5}$ and O_3 concentrations would be compared and comprehensively analyzed. By extracting the onshore wind period at an hourly level, the impact of onshore winds on the transportation of ship emissions would be further quantified. The specific structure of this study is described as follows:

The Introduction section succinctly presents the research background and objectives, including a review of the relevant literature on the impact of ship emissions. The second section of this paper serves as the Materials and Methods section, which describes the method and data used to investigate the impact of ship emissions on air quality, including a description of the adopted models, the scenario settings, the model configurations, the emission and meteorological input data, and the validation of the simulation system. The third section presents the results of the paper, including the contribution of ship emissions to air pollutant concentrations (NO_2, $PM_{2.5}$ and O_3), and the impact of onshore wind on the contribution of ship emissions to $PM_{2.5}$ and O_3 concentrations. The last section is the conclusion of this paper, which summarizes the results of the study, demonstrates their significance, points out the limitations and provides prospects for the potential future research.

2. Materials and Methods

2.1. Study Area

The GBA region is located in the south-central part of China, adjacent to the South China Sea. It includes a complex delta formed by the accumulation of sediment brought by the Pearl River system and its tributaries in the bay of the Pearl River Estuary, as well as Hong Kong and Macau [31]. Figure 1 displays a sketch map of the study area (20.32–25.32° N latitude and 110.34–116.36° E longitude), that includes the GBA region (marked with the thick black line) and its neighboring area. The analysis of the modelling results will be conducted targeting at the GBA region and the 11 cities within this region. As shown in Figure 1, the GBA region is surrounded by mountains to the west, north and east, and it has a coastline of thousands of kilometers. With rapid industrial development, the GBA region has become one of the three major urban agglomerations in China. It is also the largest comprehensive main hub of port clusters in South China, covering three of the world's top ten ports, i.e., the Guangzhou Port, the Shenzhen Port and the Hong Kong Port [32].
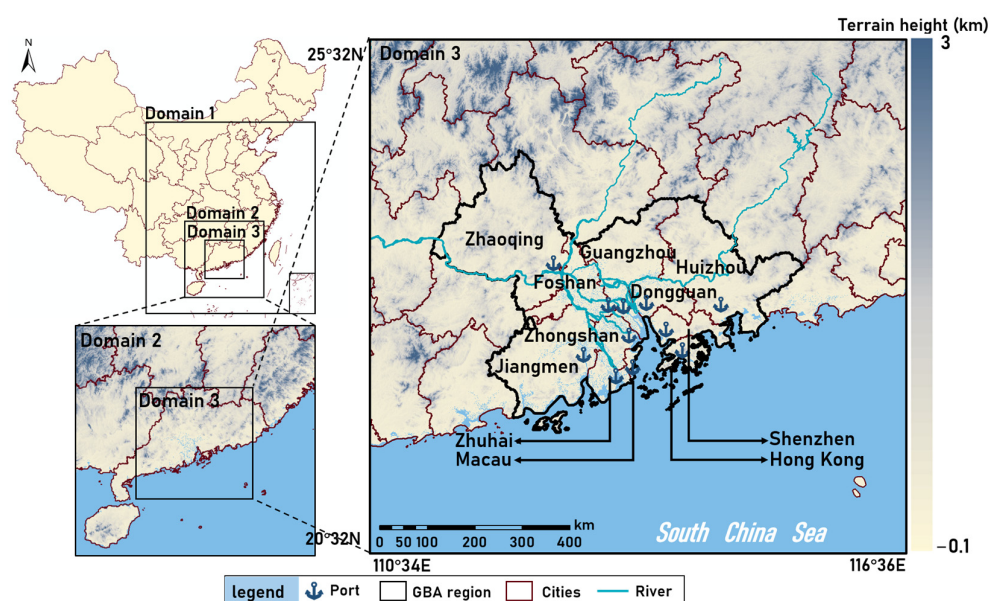

Figure 1. Sketch map of the study area.

2.2. Model Configuration and Input Data

In this study, we conducted two steps to investigate the impact of ship emissions on air quality and quantify the effect of onshore winds in the GBA in 2018. The Schematic diagram of method is shown in Figure 2. In the first step, two emission scenarios were set to simulate the contribution of ship emissions to NO_2, $PM_{2.5}$, and O_3 concentrations through the WRF/Chem model. In the second step, the onshore wind period was further extracted based on the results from the WRF model and the impact of onshore winds on pollutant transportation would be further analyzed. The scenario setting, model configuration, and input data are described in the details of the following subsections.
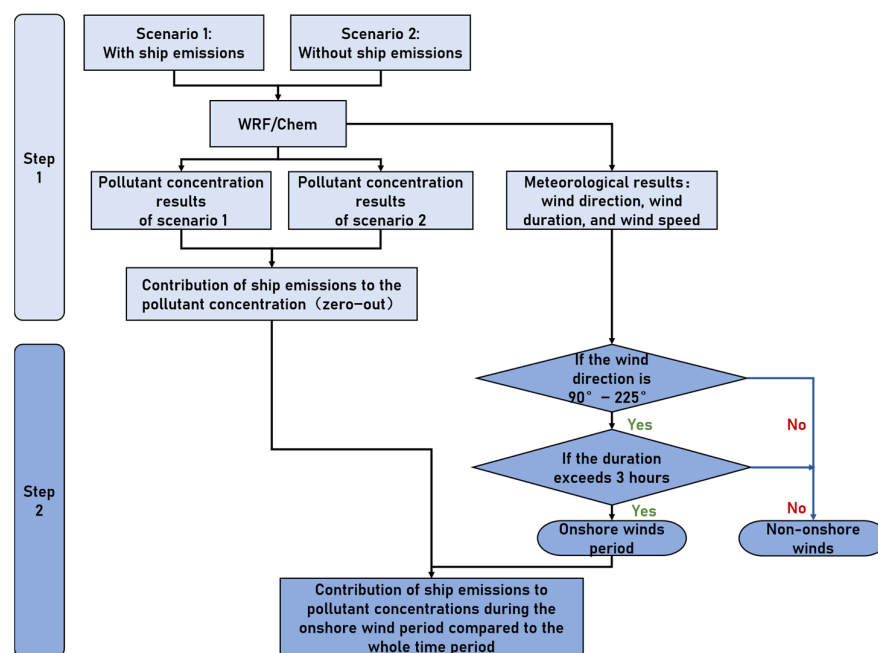
Figure 2. Schematic diagram of method.

2.2.1. Scenario Setting

The WRF/Chem model was carried out for the whole months of January, April, July and October in 2018. The emission settings of the two simulation scenarios ("With ship emissions" and "Without ship emissions") are shown in Table 1. All parameter settings were kept the same for the two simulation scenarios, except for the different emission source inputs. The "With ship emissions" scenario contains five categories of the anthropogenic emission sector from the MEIC (Multi-resolution Emission Inventory of China), the biogenic emission, the biomass emission and the ship emission; while the "Without ship emissions" scenario holds other emissions constant and set ship emissions to zero. The difference between the results of the two scenarios allows an assessment of the contribution of ship emissions to air pollutant concentrations. This method is regarded as the "zero-out" method.

Table 1. Emission inventories in the simulation scenarios.

| Scenario	Emission Inventory
With ship emissions	MEIC (Industry, power, resident, agriculture, transportation) + biogenic emission + biomass emission + ship emission
Without ship emissions	MEIC (Industry, power, resident, agriculture, transportation) + biogenic emission + biomass emission

2.2.2. Model Configuration

The WRF/Chem model developed by the U.S. National Oceanic and Atmospheric Administration (NOAA) has been extensively used by many researchers to simulate the regional air pollution [33–38]. It has the advantage of allowing online calculations of dynamic inputs (e.g., wind, temperature, the boundary layer and clouds), transportation (e.g., advection, convection and diffusion), dry deposition, gas phase chemistry, as well as radiation and photolysis rates [39–41]. Our previous studies have also applied the WRF/Chem model many times to evaluate the contribution of ship emissions to the air pollutants [27,28,42]. In this study, we followed most of the previous model configurations [11,27] to evaluate the evolution of ship emissions to the atmosphere against the background of onshore wind in the GBA region. A three-level nested-grid architecture was used to implement the WRF/Chem model (Figure 1): Domain 1 covers most of China with a grid resolution of 27 km × 27 km (96 columns and 108 rows); Domain 2 covers most of Southern China with a grid resolution of 9 km × 9 km (135 columns and 129 rows); Domain 3 covers the GBA region and adjacent areas with a grid resolution of 3 km × 3 km (207 columns and 198 rows). In the vertical dimension, 30 vertical layers were set per domain, extending from the surface to the 100 h Pa level, in which 18 vertical layers were within 4 km above the ground and the lowest layer had a thickness of about 40 m. The Regional Acid Deposition Model version 2 (RAMD2) [43] was chosen as the gas-phase chemistry mechanism and included 158 reactions from 36 species. The Model Aerosol Dynamics Model for Europe (MADE/SORGAM) [44,45] was used to calculate aerosol chemistry. The Yonsei University (YSU) [46], Eta Geo Physical Fluid Dynamics Laboratory (GFDL) [47], and Goddard [48] and Purdue Lin Noah [49,50] were selected for the Planar Boundary Layer (PBL), longwave radiation (LW), shortwave radiation (SW), and Microphysics Land surface Model scenarios, respectively. Detailed descriptions of the WRF/Chem configurations were listed in our previous studies [11,28].

2.2.3. Input Data

The meteorological input for the WRF/Chem model was derived from the National Centers for Environmental Prediction (NCEP) Global Data Assimilation System (GDAS) Final Analysis (FNL) data with a 0.25° × 0.25° spatial resolution and a temporal resolution of 6 h [51].

The ship emissions in the GBA region of 2018 were extracted from a national-scale high-spatiotemporal-resolution ship emission inventory introduced in our previous work [52], which was developed based on the ships' Automatic Identification System (AIS) big data. The total emissions of different pollutants from ships in the study area are 2.73×10^5 t (SO_2), 5.95×10^5 t (NO_x), 4.25×10^4 t ($PM_{2.5}$), 4.62×10^4 t (PM_{10}), 3.92×10^4 t (HC) and 8.69×10^4 t (CO), respectively, in 2018. Figure 3 illustrates the spatial distribution and monthly variation of ship emissions of NO_x in the GBA region and the emissions of six pollutants from ship emissions. It can be seen that the emission intensity is notably higher on the main channel, including both the offshore channel and the Pearl River waterway system. Ship emissions are lower in July, partly due to the three-and-a-half-month fishing moratorium in the South China Sea, during which fishing vessels cease operations to protect fish reproduction.

The land-based anthropogenic emissions (2017) were obtained and processed from the MEIC, (accessed on 02 March 2022) [53–59]. The biomass burning emissions developed by Zhou et al. [60] were incorporated in this study. The biogenic emissions were calculated by online version of the Model of Emissions of Gases and Aerosols from Nature (MEGAN) [61], based on the United States Geological Survey (USGS) land-use classification.
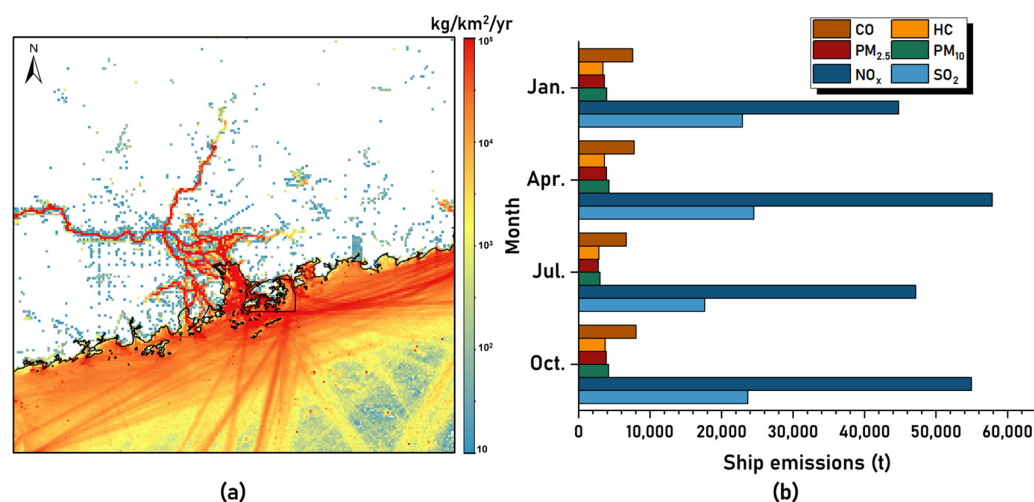
Figure 3. Overview of ship emissions in the GBA region in 2018. (**a**) Spatial distribution of annual NO$_x$ emissions from ships. (**b**) Ship emissions of different pollutants in typical months.

2.3. Model Evaluation

To evaluate the modeling performance, the simulation data resulting from the WRF/Chem was compared to the observation data obtained from monitoring stations for the four months. The meteorological variables including 2 m temperature (T$_2$), 2 m relative humidity (RH$_2$), 10 m wind speed (WS$_{10}$) and 10 m wind direction (WD$_{10}$) were compared with hourly ground-based meteorological observations from stations in the GBA region (Figure 4), in which the observations were obtained from the National Climate Data Center (NCDC) [62]. Table 2 summarizes the meteorological performance statistics of the model, including the mean bias (MB), mean absolute error (MAE), normalized mean Bias (NMB), normalized mean error (NME), and the associated correlation coefficient (R). It should be noted that the related correlation coefficient (R) formulae for wind direction differ from those for other scalars due to their vectorial nature. Thus, we followed the work of Kwok et.al [63] to compare the observation data of wind direction with the simulated values. In general, the simulation results agree with the observations with a correlation coefficient of 0.64–0.83 (statistically significant at the 95% confidence level). The MB gave reasonable results for temperature (−0.93–4.38), relative humidity (−9.51–11.79), wind speed (−0.09–0.93) and wind direction (−10.18–5.25), while the MAE was relatively higher for wind direction (12.38–18.28) compared to temperature (0.16–4.69), relative humidity (10.31–14.76) and wind speed (0.98–3.88). These values fulfil the acceptable range by Zhang et.al [64].

To further evaluate model performance for air pollutants, a comparison of modelled and observed NO$_2$, O$_3$ and PM$_{2.5}$ concentrations (hourly) for 20 sites in the GBA region is conducted, as shown in Table 3. The observed concentration of air pollutants was collected from the local Environmental Protection Bureau. As shown in Figure 4 these monitoring sites are relatively evenly distributed in multiple cities. The air quality modelling performance of WRF/Chem was evaluated using several key statistical performance indicators recommended by the U.S. Environmental Protection Agency [65], including normalized mean Bias (NMB), normalized mean error (NME), mean fraction deviation (MFB), mean fraction error (MFE) and the correlation coefficient (R) between modelled and observed concentrations. It can be seen that the correlation coefficients R for NO$_2$, O$_3$ and PM$_{2.5}$ in these cities ranged from 0.61 to 0.79, showing a good agreement between the simulations and the observations. The NMB and NME for NO$_2$ ranged from −15.09% to 6.87% and 30.89% to 52.78%, respectively. The NMB and NME for O$_3$ ranged from −35.53% to 22.05% and 31.70% to 48.10%, respectively. The NMB and NME for PM$_{2.5}$ ranged from −32.83% to −5.78% and 30.62% to 42.08%. These results are within the modeling criteria (MFB ± 60% and MFE ± 75%) for particulate matter suggested by Boylan and Russell [66].

Table 2. Performance statistics for surface Temperature (T_2), Relative Humidity (RH_2), Wind speed (WS_{10}) and Wind Direction (WD_{10}) in four sites across the GBA region.

Statistical Factors	Month	MB [1]	MAE [2]	NMB [3] (%)	NME [4] (%)	R [5]
T_2 (°C)	January	0.02	2.42	2.12	16.08	0.83
	April	4.38	4.69	20.21	6.78	0.78
	July	−0.93	2.09	−1.05	9.49	0.75
	October	−0.14	0.16	−7.92	8.83	0.81
RH_2 (%)	January	−9.51	13.14	−12.99	18.01	0.74
	April	−6.03	13.11	−13.03	22.57	0.70
	July	6.04	10.31	8.46	14.43	0.74
	October	−11.79	14.76	−18.07	22.60	0.76
WS_{10} (m/s)	January	−0.09	0.98	−9.29	34.05	0.64
	April	0.16	1.03	5.90	38.51	0.64
	July	0.93	3.88	0.45	27.02	0.68
	October	0.66	3.65	3.96	27.65	0.71
WD_{10} (°)	January	−8.87	15.16	−13.50	21.85	0.64
	April	−4.69	18.28	−19.40	39.67	0.69
	July	5.25	12.38	2.82	43.73	0.66
	October	−10.18	15.03	−13.14	17.99	0.71

[1] MB indicates the mean bias. [2] MAE indicates the mean absolute error. [3] NMB indicates the normalized mean bias. [4] NME indicates the normalized mean error. [5] R indicates the correlative coefficient.

Table 3. Performance statistics for NO_2, O_3, and $PM_{2.5}$ concentrations at 20 sites within the study area.

| Statistical Factors	Month	NMB (%)	NME (%)	MFB [6] (%)	MFE [7] (%)	R
NO_2 ($\mu g/m^3$)	January	−15.09	33.89	10.54	25.83	0.72
	April	−6.34	52.78	13.61	39.48	0.63
	July	6.87	37.98	9.56	28.69	0.76
	October	−7.41	30.89	−2.64	27.47	0.66
$PM_{2.5}$ ($\mu g/m^3$)	January	−32.83	42.08	29.11	36.10	0.73
	April	−24.54	36.20	26.92	33.09	0.72
	July	−14.94	43.38	21.69	36.12	0.75
	October	−5.98	30.23	−8.04	24.41	0.79
O_3 ($\mu g/m^3$)	January	22.05	48.10	31.78	42.38	0.79
	April	−6.09	33.59	9.37	40.85	0.65
	July	17.94	39.55	27.63	35.39	0.76
	October	−35.53	31.70	20.36	29.16	0.66

[6] MFB: indicates the mean fractional bias. [7] MFE: indicates the mean fractional error.

As mentioned above, the simulated values are generally consistent with the observed values, although there are still some deviations. These deviations may be due to meteorological inputs, inherent uncertainties in emission inventories, and unavoidable deficiencies in meteorological and air quality models (e.g., imperfections in initial and boundary conditions).

2.4. Identification of the Onshore Wind

To study the influence of the onshore wind on ship pollution, it is first necessary to establish onshore wind criteria applicable to the GBA region. According to the method proposed by Sethuraman and Rayno [67], the wind direction is classified into three categories: onshore, offshore and alongshore. As the coastline in the GBA region (marked as AB in Figure 4) is oriented at approximately east-west at about 67.5–247.5°, the classification criteria in this study are defined as follows: (1) winds ranging from 90° to 225° through 180° (E-SW) were considered onshore winds, (2) those ranging from 45° to 292.5° were considered offshore winds (NE-WNW), and (3) the rest were alongshore winds.

Since this study has a particular focus on the role of onshore winds, we combine the offshore and the alongshore winds as non-onshore winds, following Ma et al. [28]. In order to avoid sudden changes in wind direction influencing the results, we selected periods of onshore winds lasting more than 3 h.
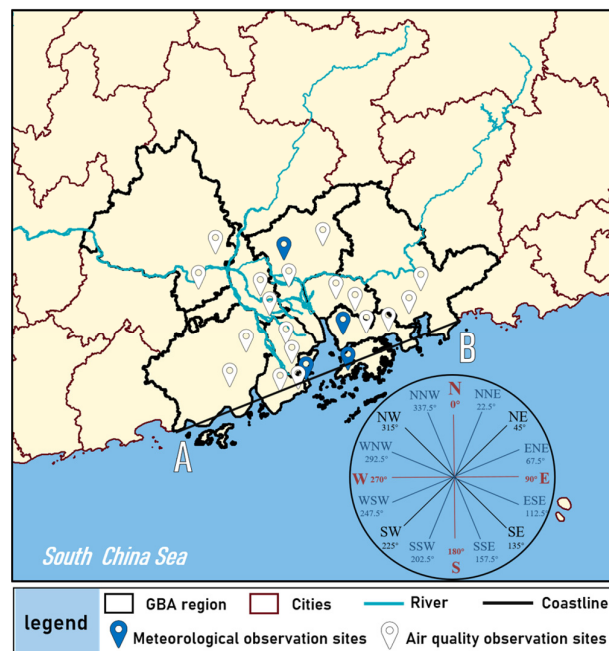
Figure 4. Schematic diagram of coastline and locations of observation sites.

Given the above criteria, we extracted the meteorological simulation results of the onshore wind period from the WRF model for different months in 2018. The total number of onshore wind occurrences was 1304 h, accounting for 44.2% of the total simulated time period (2952 h) over the duration of four months. Table 4 summarizes the occurrence times and frequencies of the onshore wind as well as the average wind speed for each month in the GBA, and Figure 5 depicts the specific occurrence time for each day. It can be seen that in the GBA, the occurrence frequency of onshore winds is higher in April and July and lower in January and October. This is because the GBA region is located at low latitudes, which is close to the tropics and has a subtropical climate. Affected by the East Asian monsoon in July, the onshore winds occur constantly with a majority from the South China Sea and the Western Pacific. In January and October, in contrast, the winter monsoon blows mostly from inland as an onshore wind. Moreover, the diurnal lasting time of the onshore winds in April and July is also longer. In these months, with an earlier sunrise, stronger solar radiation, and more rapid land warming, the temperature difference between land and sea formed earlier and could be more pronounced, promoting the formation and duration of onshore winds. However, in January and October, the solar radiation becomes weaker and the temperature difference between land and sea is smaller than that in April and July, resulting in less frequent onshore winds.

Table 4. Statistics of onshore winds in four months in 2018.

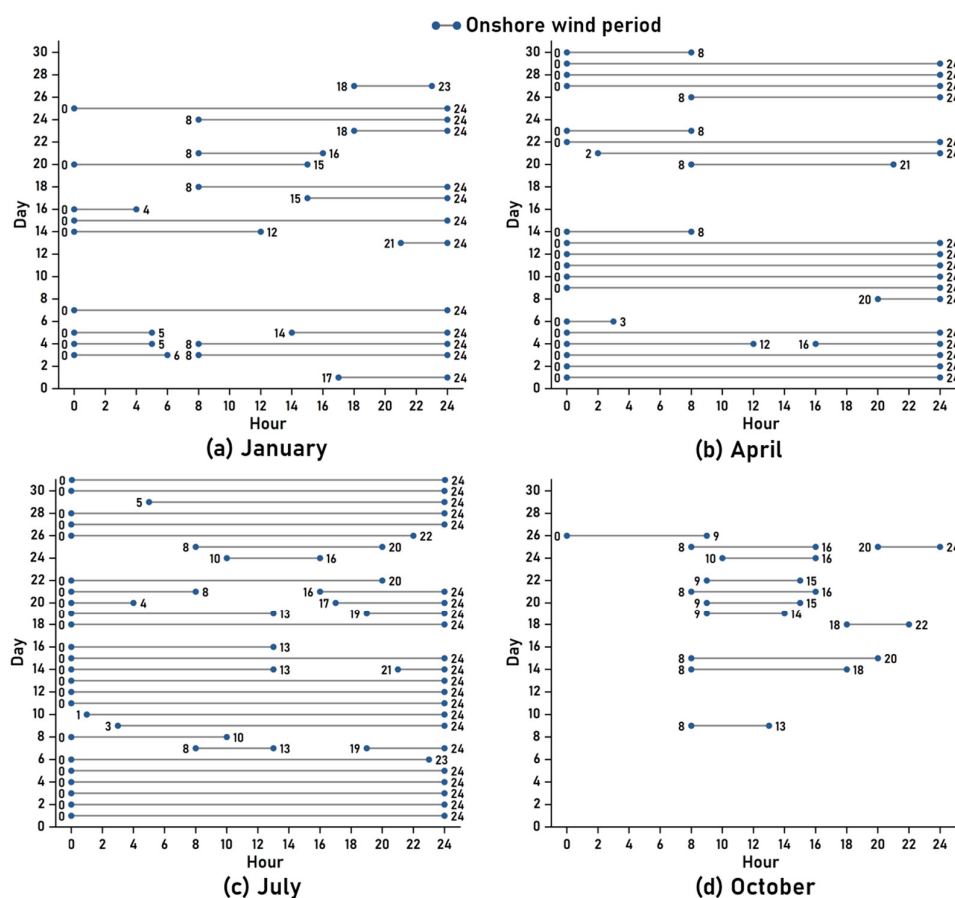| Month	Occurrence Frequency (hours)	Occurrence Frequency (%)	Average Wind Speed (m/s)	Average Wind Direction (°)
January	231	31.0	3.2	112.3
April	414	57.4	2.6	167.5
July	576	77.3	3.4	198.3
October	83	11.2	3.1	98.7

**Figure 5.** Onshore wind moment diagram in different months of 2018 in GBA region.

3. Results and Discussion

3.1. Contribution of Ship Emissions to Air Pollutant Concentrations

3.1.1. Annual Contribution

Figure 6 shows the distribution of the annual contribution of ship emissions to atmospheric NO_2, $PM_{2.5}$ and O_3 concentrations in the GBA for the year 2018, which is averaged by that of the four representatives (January, April, July, and October). Among the three criteria of air pollutants, the NO_2 concentration in the GBA was more notably affected by ships, with an annual increase of 7.4 µg/m^3 due to ship emissions. The contribution of ship emissions to the annual NO_2 concentrations estimated in this study is approximately 1.5 times that found by Chen et al. [42] targeting the PRD, and the contribution could potentially be twice as large. This is mainly because the amount of ship emissions has increased from 2014 (Chen et al.'s study [42]) to 2018 (this study), e.g., 30% for NO_x, which was accompanied by the decrease in other anthropogenic emissions, ultimately leading to an increase in the contribution rate of ship emissions. Moreover, this study includes Hong Kong and Macau besides the 11 cities in the PRD in terms of the target area, where the atmospheric environment is highly affected by ship emissions, thus the average contribution from ships was elevated regarding the whole GBA. The increase in NO_2 concentrations not only located in coastal routes and port areas where ship activities are more intensive but also in inland cities, such as Zhaoqing, etc. Besides the diffusion of NO_x emitted from river ships sailing in the Pearl River system, the transportation of pollutants from coastal ships under the influence of the onshore winds could be another reason causing the ship pollution in the inland region.
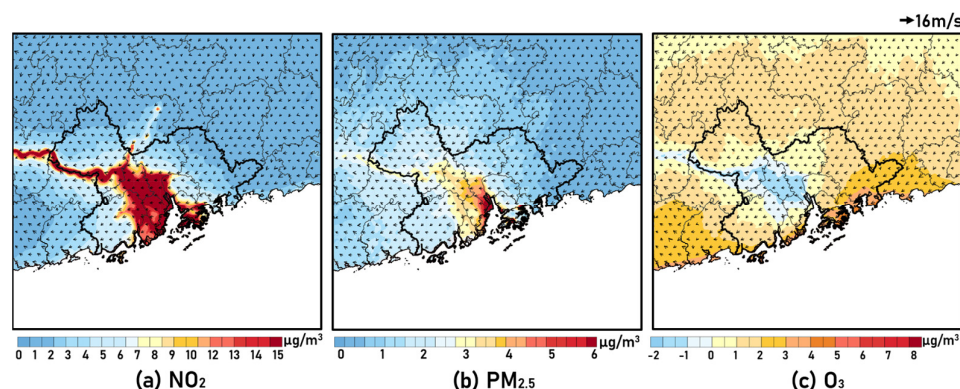
Figure 6. The annual mean contributions of ship emissions to the atmospheric concentrations of (**a**) NO_2, (**b**) $PM_{2.5}$ and (**c**) O_3.

Ship emissions also had a significant impact on $PM_{2.5}$ concentrations in this region, with an annual increase of 1.9 $\mu g/m^3$. Compared to NO_2, the contribution of ship emissions to atmospheric $PM_{2.5}$ concentration is more widespread, potentially affecting cities north of Zhaoqing. This is because atmospheric $PM_{2.5}$ has regional and composite characteristics [68]. Firstly, $PM_{2.5}$ has a long lifespan [69] and can remain in the atmosphere for an extended duration, during which it may be transported by wind to inland areas. These can be considered the "regional characteristics" of ship-induced $PM_{2.5}$ pollution. Secondly, primary pollutants such as SO_2 and NO_2 emitted by ships can be transformed into components of secondary $PM_{2.5}$ through chemical reactions (photochemical reactions, atmospheric aerosol reactions, etc.) in combination with local pollutants, which can be regarded as its "composite characteristics". In addition, this fraction of $PM_{2.5}$ can be transported further inland under the influence of "regional characteristics". Under the interaction of the above two characteristics, ship emissions play a significant role in contributing to $PM_{2.5}$ concentrations, with broad and far-reaching effects.

In terms of O_3, the annual contribution from ship emissions to O_3 concentrations in the GBA is only 0.9 $\mu g/m^3$, which shows significant spatial heterogeneity, i.e., with both positive and negative effects. In regions such as the outlying area of the GBA, ship emissions have a positive effect on O_3 concentrations. This is partly due to the interaction between a large amount of NO_x emissions from local ships and VOC (volatile organic compound) from ships or other land-based sources, or due to O_3 already produced by chemical reactions at sea and then transported to coastal cities by onshore winds. However, in the central GBA, such as the south of Guangzhou and Foshan, ship emissions appear to have a negative effect on O_3 concentrations, which largely coincides with regions where ship emissions contribute high values to NO_2 concentrations. Since the formation of O_3 has significant spatiotemporal changes due to its non-linear relationship with precursors VOC and NO_x [70,71], the detailed impact of ship emissions on O_3 concentration will be specifically analyzed in the following sections.

To further identify the regional differences, we quantified the annual contribution of ship emissions to air pollutant concentrations in different cities in the GBA, as shown in Figure 7. It can be seen that the coastal cities (cities with the exception of Zhaoqing and Foshan) are more affected by ship emissions, with more notable concentration increments of the three pollutants. In terms of NO_2 and $PM_{2.5}$, Macau is the city suffering the most severe ship-induced air pollution among the 11 cities, with concentrations rising up to 29.8 $\mu g/m^3$ and 5.9 $\mu g/m^3$, respectively. The contribution of ship emissions to NO_2 and $PM_{2.5}$ concentrations is also significant in Hong Kong, Zhongshan, and Zhuhai compared to other cities. On the one hand, these cities have abundant harbor resources, thereby experiencing high maritime traffic. As a result, pollutants emitted by ship emissions engender a pronounced impact on these urban areas. On the other hand, the above cities are situated in proximity to the South China Sea, and ship emissions generated at sea would be frequently transmitted to these cities, thus further increasing the contribution of ship

emissions to the concentration of air pollutants in these areas. In Hong Kong and Macau, where overall air pollution levels are relatively low, ship emissions have emerged as a significant problem, which has also been pointed out by some local source apportionment results [72].
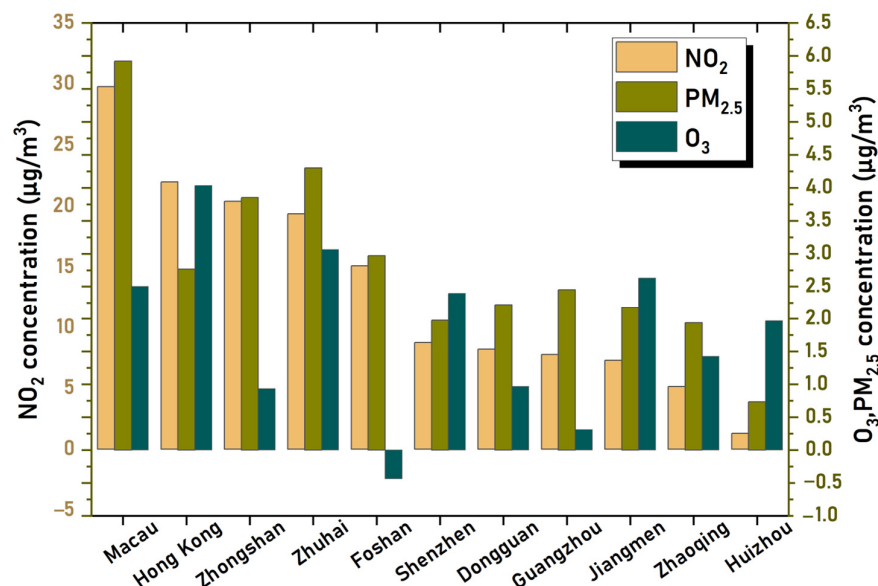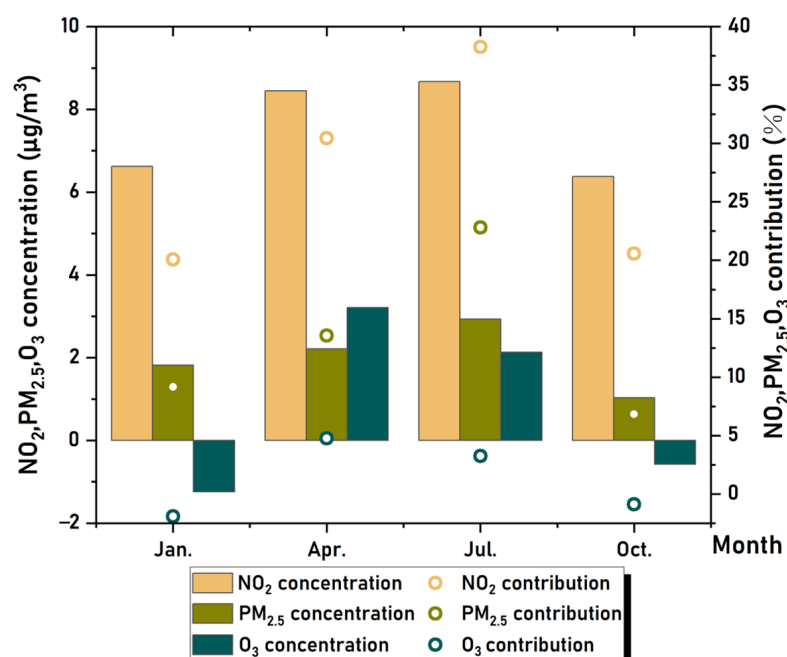

Figure 7. Contribution of ship emissions to pollutants in different cities in the GBA, the legend on the left shows NO_2 and the legend on the right shows $PM_{2.5}$ and O_3. Columns are arranged from the highest to lowest NO_2 concentrations.

In terms of O_3, however, Hong Kong turns out to be the city with the highest contribution of ship emissions to its concentrations (4.0 μg/m^3), followed by Zhuhai (3.1 μg/m^3). Although ship emissions make a substantial contribution to the concentration level of NO_2 and $PM_{2.5}$ in Guangzhou, Zhongshan, Foshan, and Dongguan, their contributions to O_3 concentrations in these cities are relatively small, and even negative, such as in Foshan (−0.5 μg/m^3). In contrast, in Huizhou, the ship emissions contribute less to NO_2 and $PM_{2.5}$ concentrations but contribute to comparatively large O_3 concentrations. This is because Guangzhou, Zhongshan, Foshan and Dongguan are typical industrialized and commercial concentration areas, most of which are in a VOC-limited regime, and the increase in NO_x emissions from ships will reduce the O_3 concentrations [73,74]; while Huizhou is a relatively clean city in which O_3 generation is more sensitive to NO_x [75–77], and thus the O_3 concentration could be easily raised up with the increase of ship emissions. Therefore, it is essential to fully account for the O_3 generation mechanism while controlling ship emissions within the GBA and to develop accurate, scientifically supported control methods that are specific to each city.

Zhaoqing is an inland city within the GBA region, yet even there, the influence of ship emissions is still not negligible. On the one hand, the port of Zhaoqing, located in the lower reaches of the Xijiang River, a prime waterway in the Pearl River system, still carries a large amount of ship activity in the GBA region. On the other hand, ship emissions from the southeast can be frequently transported to the northwest under the influence of wind, and secondary reactions continuously occur during the transportation process, leading to the increment in concentrations of NO_2, $PM_{2.5}$ and O_3 in Zhaoqing. Therefore, the impact of ship emissions, including both local contribution and regional transportation, should also be taken into consideration when formulating emission reduction measures to improve air quality in inland cities.

3.1.2. Monthly Variation

The contribution of ship emissions to NO_2, $PM_{2.5}$ and O_3 concentrations in different months in the GBA region are shown in Figure 8, and their spatial distribution is shown in Figure 9. Despite the fact that the GBA is located at low latitudes where seasonal variations are less pronounced than that at mid and high-latitudes, significant monthly differences were observed regarding the impact of ship emissions on air quality. Regardless of the type of pollutant, the average contribution of ship emissions to its concentration in April and July is greater compared to January and October. For NO_2 and $PM_{2.5}$, the contribution of ship emissions to their concentrations in the GBA peaked in July, at 8.7 $\mu g/m^3$ (38.2%) and 2.9 $\mu g/m^3$ (22.8%), respectively, which are 1.3 times and 2.9 times that of October, respectively. The inter-month variation in ship emissions and meteorological factors (especially wind direction) are the main reasons for the differences in the ship contributions. In April, the relatively high ship emissions encounter the predominantly southeast wind in the GBA region, facilitating the transportation of ship pollutants to the northern inland areas. In July, although ship emissions are lower compared to April, the prevailing winds from the south (Figure 9) are more favorable for the transportation of ship pollutants to inland areas, resulting in even higher ship contributions. In contrast, in January and October, when the wind direction is mainly north and northeast, ship pollutants are transported to sea. Thus, even though ship emissions in October are higher than that in July, their contribution to pollutant concentrations becomes lower.

Figure 8. The mean concentration and contributions of ship emissions in the four months.

Compared to NO_2 and $PM_{2.5}$, the impact of ship emissions on O_3 pollution in different months is more complicated. Although the annual contribution of ship emissions to the O_3 concentration in the targeted 11 cities is only 0.9 $\mu g/m^3$, it shows notable monthly variations. Statistics indicate that ship emissions led to an overall increase in O_3 concentrations in April (3.2 $\mu g/m^3$, 4.8%) and July (2.1 $\mu g/m^3$, 3.2%), respectively, but a decrease in January (−1.3 $\mu g/m^3$, −2.0%) and October (−0.6 $\mu g/m^3$, −0.9%), respectively (Figure 8). On this basis, the bifold impact of ship emissions on O_3 concentration appears in all months and shows notable spatial variation in different months. As shown in Figure 9c, the negative contribution of ship emissions to O_3 concentrations was observed in all four months of which the extent was wider in January and October, encompassing nearly all cities except for Huizhou. In the study on the monthly average contribution of ship emissions to O_3 concentrations, Chen et al. [14] found that the contribution of ship emissions to O_3

concentrations in the PRD region in July 2015 was 1.9 μg/m^3, which in this study was 2.1 μg/m^3, slightly higher than the study by Chen et al. [14]. This is due to the fact that NO$_x$ emissions from ships were greater in 2018 than in 2015, and in July most of the cities in the region are in the NO$_x$ control area, meaning the larger amount of NO$_x$ emissions from ships leads to a higher O$_3$ concentration contribution.
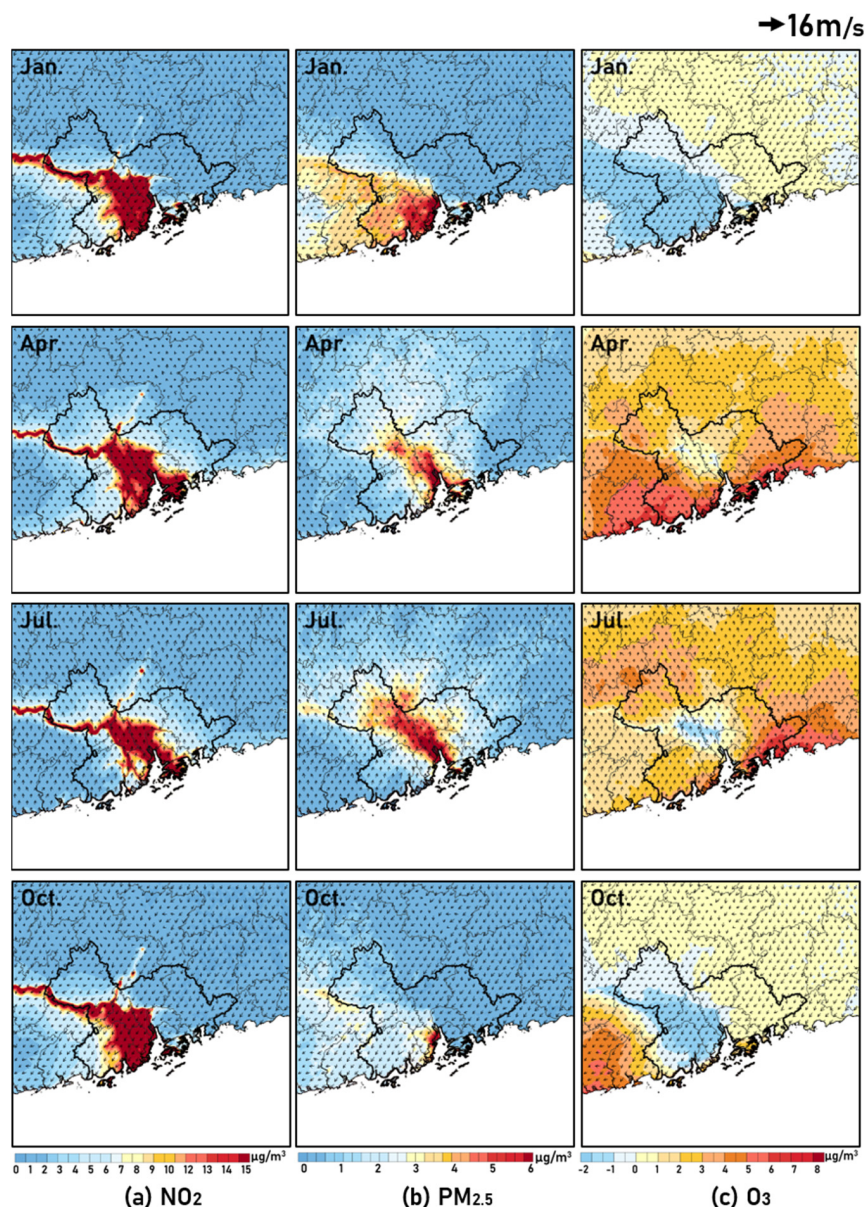
Figure 9. The contributions of ship emissions to the (**a**) NO$_2$, (**b**) PM$_{2.5}$ and (**c**) O$_3$ in January, April, July, and October in the GBA region in 2018 (μg/m^3). The target cities for calculation are encompassed by the black bold curve.

　　Besides the influence of wind direction (as analyzed above), the spatiotemporal distribution of O$_3$-sensitive areas could better explain the variation in the contribution of ship emissions to O$_3$ concentrations. The lower temperature in January and October reduces the volatility of the VOC, and when the concentration of VOC in the atmosphere has been reduced, this leads to an increase in the NO$_x$/VOC ratio. With a weaker VOC cycle relative to the NO$_x$ cycle, the majority of O$_3$ generation in most areas of the GBA regions is a VOC-limited regime [78,79]. Thus, ship emissions with large amounts of NO$_x$ would reduce the concentration of ozone under the frequent titration effect of NO on O$_3$, especially in the western area of the GBA. In contrast, during the warmer months of April and July,

active photochemical reactions lead to a shorter NO_x lifetime and higher volatility of VOC. This results in higher VOC/NO_x ratios compared to January and October. Along with some areas shifting from a VOC control region to synergistic control or the NO_x control regions, the ship emissions with abundant NO_x would ultimately lead to an increase of the O_3 concentration [80].

3.2. Impact of Onshore Wind on the Contribution of Ship Emissions to Air Pollutant Concentrations

Onshore winds play an important role in the diffusion and transportation of pollutants in coastal areas [25,81,82]. In regions with high ship emission intensity, the onshore winds can induce pollutants emitted from ships transported to inland areas [10,26], leading to more severe air pollution. However, the levels and characteristics of the impact of onshore winds have been qualitatively investigated in previous studies less regarding the ship-induced air pollution in the GBA [72,83]. To conduct a more in-depth investigation into this matter, this study explores the impact of onshore winds on the contribution of ship emissions to air pollutant concentrations including both $PM_{2.5}$ and O_3, by examining the wind direction on an hourly scale for four representative months in 2018 and screening the simulation results for periods with more than 1300 h of onshore winds. Results will be analyzed through both a temporal and spatial perspective.

3.2.1. $PM_{2.5}$ Pollution
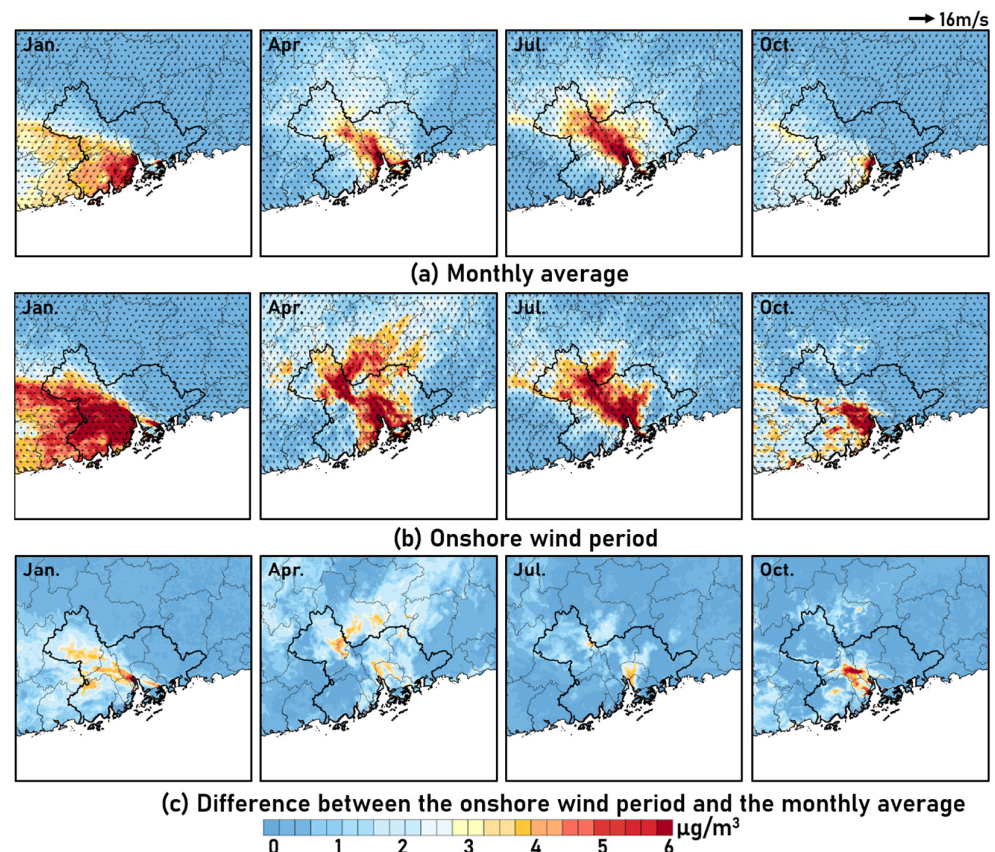
Figure 10 shows the contribution of ship emissions to $PM_{2.5}$ concentrations for monthly averages during the onshore wind hours and the differences between them. The contribution of ship emissions to the annual $PM_{2.5}$ concentrations during onshore wind periods in the GBA region was 0.9 $\mu g/m^3$ (1.5 times) higher than the annual average. This amplified effect of ship-induced $PM_{2.5}$ pollution by onshore winds has also been reported in the YRD region, with similar ratios of 1.8–2.7 times over four months [10]. However, Lv et al.'s study [10] used the average daily wind direction as the condition for determining the onshore wind days, while this study determined the onshore winds on an hourly scale. This finer temporal resolution may result in a more accurate quantitative evaluation of the impact of onshore winds on pollutant transportation.

For all months, the contribution of ship emissions to inland $PM_{2.5}$ concentration would be more significant under the influence of onshore winds, but there are differences in the affected areas. In January and October, as the onshore wind mostly comes from the east or southeast, the onshore airflow carrying $PM_{2.5}$ is mostly transported to the northwest of the GBA, resulting in the high-value area of ship-contributed $PM_{2.5}$ mainly gathered in the western part of the study area such as Zhongshan and Foshan. In January, the contribution of ship emissions in Zhongshan and Foshan can even reach 7.7 $\mu g/m^3$ and 5.5 $\mu g/m^3$. In April and July, the onshore winds were mostly from the south, thus, the onshore airflow carrying $PM_{2.5}$ was mostly transported to the north of the study area, resulting in the expansion of the area significantly affected by ship emissions to a more distant area in the north. During the onshore wind hours, the contribution of ship emissions to $PM_{2.5}$ reaches 5.6 $\mu g/m^3$ in Dongguan, which is located in the northern part of the study area. It is worth pointing out that, in July, although the contribution of ship emissions to $PM_{2.5}$ increases in the central part of the GBA during the onshore wind hours (up to about 3.7 $\mu g/m^3$), the contribution of ship emissions in the whole GBA is lower than the monthly average, with a small difference of 0.1 $\mu g/m^3$. The reason for this phenomenon may be that, although the frequency of onshore winds is the highest in July (up to 77.3%), which will transport ship emissions to inland areas frequently, the contribution of ship emissions to $PM_{2.5}$ concentrations is somewhat weakened by the fact that summer onshore wind periods are more often accompanied by precipitation. In April and October, the differences in the spatial distribution of the ship-contributed $PM_{2.5}$ were more significant compared to January and July. During the onshore wind hours, the impact of ship emissions can penetrate further inland: in April, the range of ship contributions to $PM_{2.5}$ exceeding 4.0 $\mu g/m^3$ extends to

the area north of Guangzhou; in October, the range of ship contribution to $PM_{2.5}$ exceeding $4\ \mu g/m^3$ extends to the western part of the GBA. This is a significant expansion compared to January and July.

Figure 11 further summarizes the differences in the contribution of ship emissions to $PM_{2.5}$ concentrations in 11 cities in the GBA region during the onshore wind period compared to the whole time period. It can be seen that during the onshore wind period, the contribution of ship emissions to $PM_{2.5}$ concentration is much higher than the annual average in all cities except Macau and Zhuhai. The cities with the largest increase during the onshore wind period are Zhongshan and Foshan, with an increase of 1.9 and 1.5 $\mu g/m^3$, respectively. The city with the smallest difference is Huizhou, which increases by only $0.2\ \mu g/m^3$. This is because in the GBA, the annual average wind direction of the onshore wind is southeastward, and Zhongshan and Foshan are located in the west of the GBA area, in the downwind zone, so these two cities are more affected by ship emissions. Huizhou, on the other hand, is located in the southeastern part of the GBA region and is in the upwind direction, so it is less affected. In contrast, Macau and Zhuhai show a higher annual average contribution than the contribution during the onshore wind, where the contribution of ship emissions to $PM_{2.5}$ concentration is 0.8 $\mu g/m^3$ and 0.4 $\mu g/m^3$ lower than the annual average. This can be attributed to the fact that these two cities are located on the two sides of the Pearl River Estuary respectively, which are influenced by ship emissions in both offshore and onshore winds (even when the offshore winds are blowing, the emissions from ships in the Pearl River Estuary are transported to these two cities).
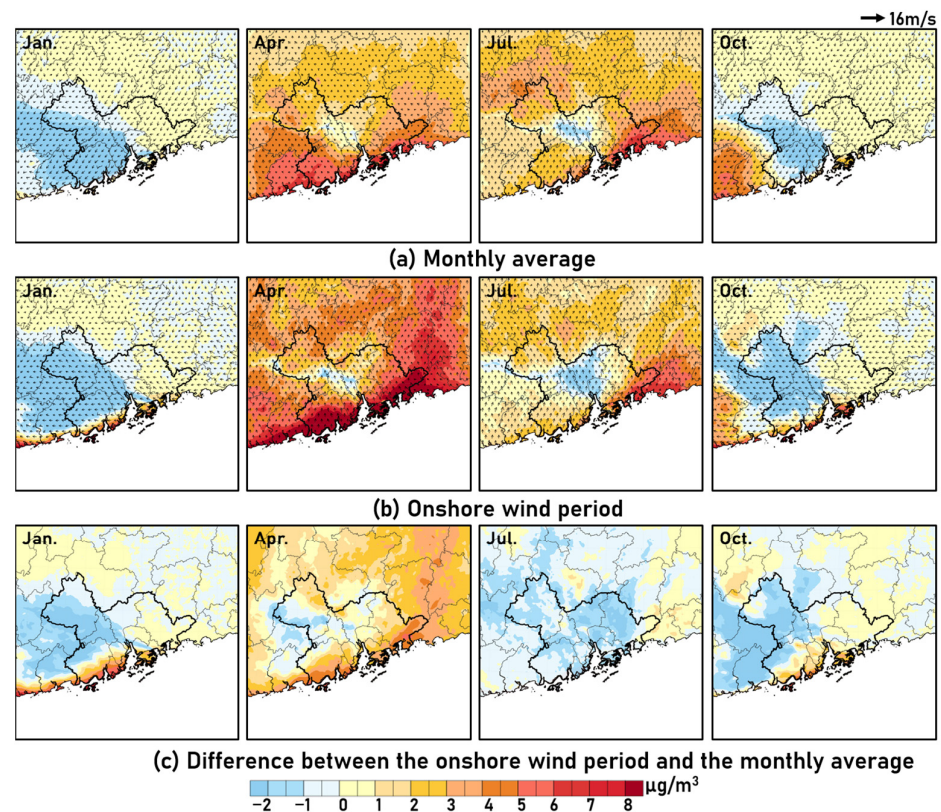

Figure 10. The contribution of ship emissions to $PM_{2.5}$ concentrations for monthly averages (**a**), during the onshore wind hours (**b**), and the differences between them (**c**), in January, April, July and October.
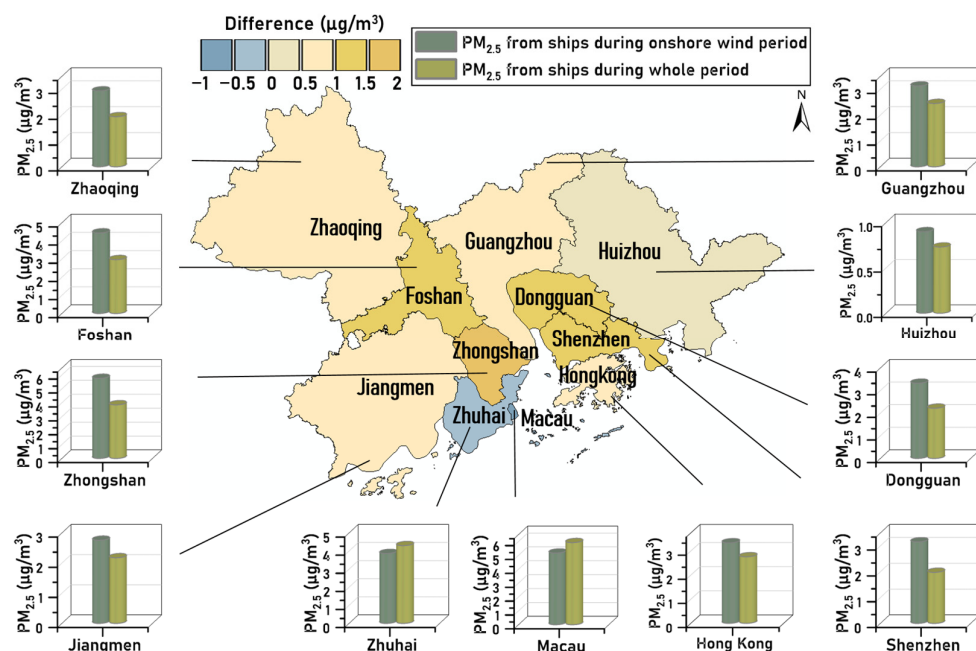
Figure 11. The differences in the contribution of ship emissions to PM$_{2.5}$ concentrations in 11 cities in the GBA region during the onshore wind period compared to the whole time period.

3.2.2. O$_3$ Pollution

Compared to PM$_{2.5}$, the effect of onshore winds on the contribution of ship emissions to O$_3$ concentrations is more complex. Figure 12 shows the average contribution of ship emissions to O$_3$ and its difference from the monthly average for different months. It is found that the contribution during the onshore wind period shows different trends in different months. The common point for all months is that the contribution during the onshore wind period shows a trend of negative areas expanding inland. This is because under the influence of onshore winds, the NO$_x$ plume from ship emissions is transported to the downwind region, raising the NO$_x$/VOC ratio in the downwind region and thus causing ozone production more sensitive to VOC [84]. The difference is that in January, July, and October, onshore winds exacerbate the decreasing trend of the contribution of ship emissions to O$_3$, decreasing by 0.1, 0.9, and 0.2 μg/m^3 compared to the monthly average, while in April, onshore winds raise the contribution of ship emissions to O$_3$ concentrations by 1.5 μg/m^3. The reason for this situation is that in January and October, most of the GBA is in the VOC-control area [78,79], thus the ozone concentration decreases with the frequently ship-emitted NO$_x$ transported inland during the onshore wind hours. As a result, the negative contribution to the O$_3$ concentration from ship emissions decreases further, while the area of negative value becomes larger. In April, the large area of outlying cities in the GBA changed from the VOC control area to the NO$_x$ control area or synoptic control area, as reported by Itahashi et al. and Liu et al. [78,79], causing the concentration of O$_3$ to increase with its precursors. Thus, the transportation of NO$_x$ emitted from ships to inland areas under onshore wind hours will lead to a higher O$_3$ concentration. It is worth noting that in July, although the average contribution of ship emissions to O$_3$ is positive, onshore wind reduced this contribution. Moreover, the ship-contributed O$_3$ concentration even becomes negative under the influence of onshore wind in regions that originally showed positive values, such as the southern part of Guangzhou. Possible reasons for this are: (1) in July, the presence of large amounts of clouds during the onshore wind period leads to lower solar radiation, which inhibits ozone production from ozone precursors emitted by ships [85]; (2) the onshore wind brings humid air from the ocean, which is more likely to form precipitation on land during summer [86], resulting in a negative contribution of ship emissions to O$_3$ concentrations.

Figure 12. The contribution of ship emissions to O$_3$ concentrations for monthly averages (**a**) during the onshore wind hours (**b**) and the differences between them (**c**) in January, April, July and October.

Figure 13 further shows the contribution of ship emissions to O$_3$ in different cities under the influence of onshore winds. At the annual average level, the level of contribution of ship emissions to O$_3$ shows a significant bidirectional trend during the onshore wind, i.e., enhanced and diminished in different areas.
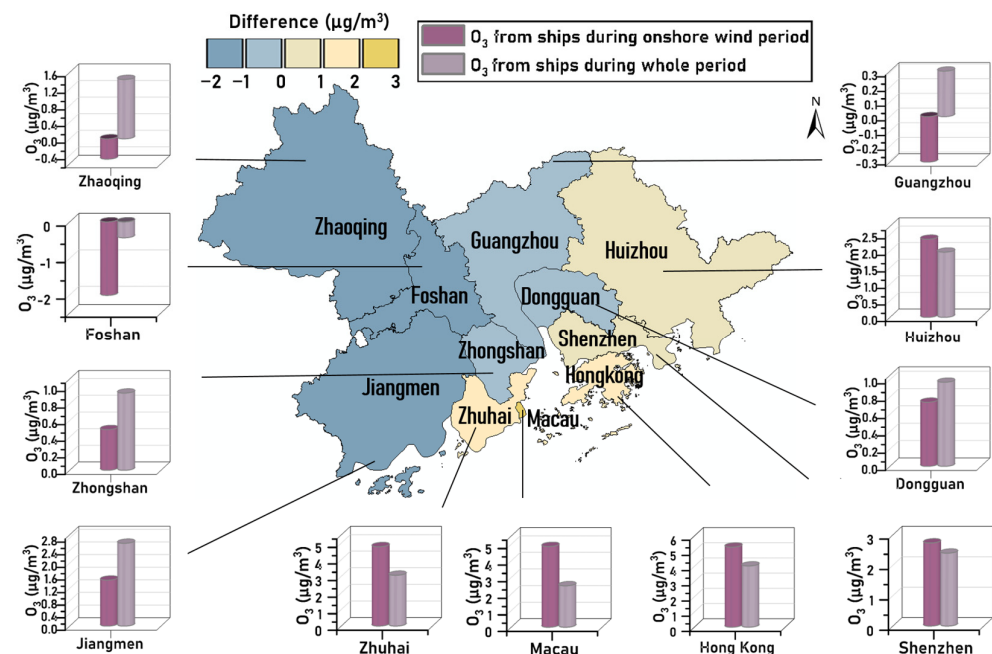
Figure 13. The differences in the contribution of ship emissions to O$_3$ concentrations in 11 cities in the GBA region during the onshore wind period compared to the whole time period.

In areas where ship emissions cause a decrease in O_3 concentrations, such as Foshan and parts of Zhongshan, Jiangmen, and Dongguan, the onshore wind intensifies this decreasing trend, and in Foshan, it can reach up to 4.6 times the average contribution. Belonging to VOC control areas, onshore winds transport NO_x from ships to these areas, which increases the local NO_x/VOC ratio and thus enhances the titration of NO to O_3, resulting in a further decrease in the contribution of ship emissions to O_3. In contrast, in areas where ship emissions contribute positively to O_3 concentrations, such as Huizhou, Hong Kong, Zhuhai, and Macau, onshore winds further increase the contribution to O_3 concentrations, reaching 1.2, 1.3, 1.6, and 2.0 times the average contribution. Since these cities are dominated by the NO_x control area, the NO_x emissions from ships transported by the onshore winds lead to an increase in the contribution to O_3 concentrations. It is noteworthy that the annual contribution of ship emissions to O_3 in Guangzhou and Zhaoqing is positive, although this contribution becomes negative during the onshore wind hours. This may indicate the potential change of the division of the O_3 sensitivity zone to its precursors under the effect of onshore winds. Therefore, we should consider not only the differences in emission structures among cities, but also the effects of meteorological conditions when developing effective control measures to improve air quality.

4. Conclusions and Implications

In this study, the WRF/CHEM model was used to investigate the contribution of ship emissions to air pollutant concentrations in the GBA for four typical months in 2018. The onshore wind, as a prominent factor, was selected separately to inspect its role on the transportation of ship-emitted emissions.

The ship emissions caused the annual concentrations of NO_2, $PM_{2.5}$ and O_3 in the GBA which increased by 7.4, 1.9, and 0.9 $\mu g/m^3$, respectively. The increase in air pollutant concentrations was especially high in coastal cities such as Macao, Hong Kong and Zhuhai. Macau is the city with the most significant ship-contributed NO_2 (29.8 $\mu g/m^3$) and $PM_{2.5}$ (5.9 $\mu g/m^3$) concentrations, while Hong Kong turns out to be the city with the highest ship-contributed O_3 concentrations (4.0 $\mu g/m^3$). The contribution of ship emissions to the O_3 concentration varies significantly among cities due to differences in ozone sensitivity. In cities where O_3 generation is mostly NO_x-limited, ship emissions contribute higher concentrations of both NO_2 and O_3 (e.g., Huizhou); in cities where O_3 generation is more often VOC-limited, ship emissions contribute high concentrations of NO_2 but low and even negative concentrations of O_3 (e.g., Guangzhou and Foshan).

The seasonal variation in the GBA is unremarkable, although, changes in the prevailing wind direction still largely affect the transportation pattern of ship emissions in different months. The contribution of ship emissions to the concentration of all three pollutants tended to be high in April and July and low in January and October. The contribution of ship emissions to NO_2 and $PM_{2.5}$ concentrations in the GBA peaked in July, at 8.7 $\mu g/m^3$ and 2.9 $\mu g/m^3$, respectively, while ship emissions led to an increase in O_3 concentrations in April (3.2 $\mu g/m^3$) and July (2.1 $\mu g/m^3$), but a decrease in January (-1.3 $\mu g/m^3$) and October (-0.6 $\mu g/m^3$). These monthly variations in ship contributions are highly relative to the emission changes, wind direction and atmospheric oxidation mechanism.

The frequent occurrence of onshore winds in the GBA facilitates the transportation of ship-emitted pollutants to inland areas, resulting in the contribution of ship emissions to the annual $PM_{2.5}$ concentrations during which onshore winds increased by 0.9 $\mu g/m^3$ compared to the annual average contribution. The cities with the highest contribution of onshore winds to $PM_{2.5}$ concentrations from ships are Zhongshan and Foshan, which had an increase of 1.9 $\mu g/m^3$ and 1.5 $\mu g/m^3$, respectively, as they are located downwind of the onshore winds. The effect of onshore winds is particularly pronounced in April and October: in April, with most of the onshore winds coming from the south, the range of ship contribution to $PM_{2.5}$ exceeding 4 $\mu g/m^3$ extends to the area north of Guangzhou; in October, with the onshore winds mostly easterly or southeasterly, the range of ship contribution to $PM_{2.5}$ exceeding 4 $\mu g/m^3$ extends to the western part of the GBA.

The contribution of ship emissions to O_3 concentrations during onshore winds appears to have a more pronounced two-way trend of a strengthening or weakening effect. In Foshan and Zhongshan (VOC-sensitive), onshore winds intensify the negative effect on the contribution of ship emissions to O_3 concentrations, with a maximum of 4.6 times (Foshan). In Huizhou (NO_x-sensitive), onshore winds also intensified the positive contribution of the ship-induced O_3 concentration. In terms of the monthly variations, the onshore winds raise the ship contribution to O_3 concentrations in April by 1.5 $\mu g/m^3$, while exacerbating the decreasing trend of the contribution in other months. The spatial and monthly variations in the effect of onshore winds in regard to the ship pollution indicate that besides the emission structures, meteorological conditions such as wind are also a vital factor for developing effective measures so as to relieve ship-induced air pollution.

Onshore winds occur more frequently in the GBA compared to mid-latitude regions, and under this influence, ship-emitted pollutants can be transported inland more frequently. Their contributions to the atmospheric $PM_{2.5}$ and O_3 pollution vary throughout the year. In addition to this, as onshore winds bring moist air from the sea, the contribution of ship emissions to $PM_{2.5}$ as well as O_3 is not always positive and may instead be reduced due to factors such as precipitation. By quantifying these effects and discussing the spatial and temporal characteristics, the role of onshore winds in the transportation of pollutants emitted from ships is highlighted, contributing to a better understanding of the current state of pollution from shipping at the coastal port scale. These results provide strong empirical results for relevant studies and provide references for similar work in other regions and ports.

With the tightening of anthropogenic emission control standards in China, increasing emission reduction efforts will result in diminishing marginal benefits. Meanwhile, unfavorable meteorological conditions have gradually become the main triggering factor for the occurrence of heavy air pollution. Therefore, the future governance of air pollution requires precise prevention and control, rather than "one size fits all" emission source control measures. Considering the variability of meteorological conditions, predicting the occurring period and intensity of onshore winds and prioritizing targeted measures for regions that may be potentially heavily affected by ship pollutants, can become one of the ways to control air pollution in coastal port areas. For this purpose, our results can not only enhance the understanding of the role of onshore winds in air pollution but also provide important references and guidance for measure formation to improve coastal air quality.

The results of our study are subject to a few limitations. Considering the nonlinear variation of O_3 concentration on its precursor emissions, the scenario setting based on a "zero-out" method would have a certain degree of uncertainties in quantifying the contribution of ship emissions on the O_3 concentrations. In addition to the bias in the emission inventory, the physical and chemical model mechanism led to unavoidable uncertainties in the results. Given the above analysis, there are still some uncertainties in the impact of ship emissions on air quality in coastal areas under the influence of onshore winds which need further and more in-depth studies. For example, it is worthwhile to further explore the effects of ship emissions on sulfur deposition and nitrogen deposition in future studies, mainly because NO_x and SO_2 are the pollutants that account for the largest share of ship emissions. Furthermore, this study finds that ship emissions contribute positively to $PM_{2.5}$ concentrations in the whole Great Bay region; however, in some cities (e.g., Zhongshan) they contribute negatively to O_3. This poses a challenge for the introduction of a synergistic $PM_{2.5}$ and O_3 emission reduction policy, and further research is necessary.

Author Contributions: Conceptualization, D.C. and Q.C.; methodology, Q.C., J.L. and Y.Z. (Ying Zhou); validation, Y.Z. (Ying Zhao) and J.H.; formal analysis, X.W. and Q.C.; data curation, Q.C.; writing—original draft preparation, Q.C.; writing—review and editing, X.W., D.C. and Q.C.; visualization, Y.M. and Q.C.; supervision, D.C., X.W. and X.G.; project administration, X.W.; funding acquisition, D.C. All authors have read and agreed to the published version of the manuscript.

Institutional Review Board Statement: Not applicable.

Informed Consent Statement: Not applicable.

Data Availability Statement: The data presented in this study are openly available in the references [51,61,62].

Acknowledgments: This paper represents the perspectives of the authors and does not necessarily represent the official views of our sponsors. We would like to appreciate the anonymous reviewers for their valuable comments and suggestions to improve the manuscript.

Conflicts of Interest: The authors declare no conflict of interest.

References

1. The State Council the People's Republic of China. Available online: http://www.gov.cn/xinwen/2021-10/04/content_5640899.htm (accessed on 10 April 2023).
2. ChineseShipping. Available online: https://info.chineseshipping.com.cn/cninfo/TodayTopNews/201504/t20150401_1250934.shtml (accessed on 10 April 2023).
3. Corbett, J.J.; Fischbeck, P.S.; Pandis, S.N. Global nitrogen and sulfur inventories for oceangoing ships. *J. Geophys. Res. Atmos.* **1999**, *104*, 3457–3470. [CrossRef]
4. Capaldo, K.; Corbett, J.J.; Kasibhatla, P.; Fischbeck, P.; Pandis, S.N. Effects of ship emissions on sulphur cycling and radiative climate forcing over the ocean. *Nature* **1999**, *400*, 743–746. [CrossRef]
5. Corbett, J.J.; Fischbeck, P. Emissions from Ships. *Science* **1997**, *278*, 823–824. [CrossRef]
6. Ramacher, M.O.P.; Tang, L.; Moldanová, J.; Matthias, V.; Karl, M.; Fridell, E.; Johansson, L. The impact of ship emissions on air quality and human health in the Gothenburg area—Part II: Scenarios for 2040. *Atmos. Chem. Phys.* **2020**, *20*, 10667–10686. [CrossRef]
7. Mölders, N.; Porter, S.E.; Cahill, C.F.; Grell, G.A. Influence of ship emissions on air quality and input of contaminants in southern Alaska National Parks and Wilderness Areas during the 2006 tourist season. *Atmos. Environ.* **2010**, *44*, 1400–1413. [CrossRef]
8. Liu, H.; Meng, Z.-H.; Lv, Z.-F.; Wang, X.-T.; Deng, F.-Y.; Liu, Y.; Zhang, Y.-N.; Shi, M.-S.; Zhang, Q.; He, K.-B. Emissions and health impacts from global shipping embodied in US–China bilateral trade. *Nat. Sustain.* **2019**, *2*, 1027–1033. [CrossRef]
9. Liu, H.; Fu, M.; Jin, X.; Shang, Y.; Shindell, D.; Faluvegi, G.; Shindell, C.; He, K. Health and climate impacts of ocean-going vessels in East Asia. *Nat. Clim. Chang.* **2016**, *6*, 1037–1041. [CrossRef]
10. Lv, Z.; Liu, H.; Ying, Q.; Fu, M.; Meng, Z.; Wang, Y.; Wei, W.; Gong, H.; He, K. Impacts of shipping emissions on $PM_{2.5}$ pollution in China. *Atmos. Chem. Phys.* **2018**, *18*, 15811–15824. [CrossRef]
11. Chen, D.; Zhao, N.; Lang, J.; Zhou, Y.; Wang, X.; Li, Y.; Zhao, Y.; Guo, X. Contribution of ship emissions to the concentration of PM(2.5): A comprehensive study using AIS data and WRF/Chem model in Bohai Rim Region, China. *Sci. Total Environ.* **2018**, *610–611*, 1476–1486. [CrossRef]
12. Zhang, Y.; Eastham, S.D.; Lau, A.K.H.; Fung, J.C.H.; Selin, N.E. Global air quality and health impacts of domestic and international shipping. *Environ. Res. Lett.* **2021**, *16*, 084055. [CrossRef]
13. Lin, H.; Tao, J.; Qian, Z.M.; Ruan, Z.; Xu, Y.; Hang, J.; Xu, X.; Liu, T.; Guo, Y.; Zeng, W.; et al. Shipping pollution emission associated with increased cardiovascular mortality: A time series study in Guangzhou, China. *Environ. Pollut.* **2018**, *241*, 862–868. [CrossRef] [PubMed]
14. Chen, C.; Saikawa, E.; Comer, B.; Mao, X.; Rutherford, D. Ship Emission Impacts on Air Quality and Human Health in the Pearl River Delta (PRD) Region, China, in 2015, With Projections to 2030. *Geohealth* **2019**, *3*, 284–306. [CrossRef] [PubMed]
15. Tao, J.; Zhang, L.; Cao, J.; Zhong, L.; Chen, D.; Yang, Y.; Chen, D.; Chen, L.; Zhang, Z.; Wu, Y.; et al. Source apportionment of PM(2.5) at urban and suburban areas of the Pearl River Delta region, south China—With emphasis on ship emissions. *Sci. Total Environ.* **2017**, *574*, 1559–1570. [CrossRef] [PubMed]
16. Lai, H.K.; Tsang, H.; Chau, J.; Lee, C.H.; McGhee, S.M.; Hedley, A.J.; Wong, C.M. Health impact assessment of marine emissions in Pearl River Delta region. *Mar. Pollut. Bull.* **2013**, *66*, 158–163. [CrossRef]
17. Wang, H.; Lyu, X.; Guo, H.; Wang, Y.; Zou, S.; Ling, Z.; Wang, X.; Jiang, F.; Zeren, Y.; Pan, W.; et al. Ozone pollution around a coastal region of South China Sea: Interaction between marine and continental air. *Atmos. Chem. Phys.* **2018**, *18*, 4277–4295. [CrossRef]
18. Zheng, Y.; Jiang, F.; Feng, S.; Cai, Z.; Shen, Y.; Ying, C.; Wang, X.; Liu, Q. Long-range transport of ozone across the eastern China seas: A case study in coastal cities in southeastern China. *Sci. Total Environ.* **2021**, *768*, 144520. [CrossRef]
19. Wang, R.; Tie, X.; Li, G.; Zhao, S.; Long, X.; Johansson, L.; An, Z. Effect of ship emissions on O_3 in the Yangtze River Delta region of China: Analysis of WRF-Chem modeling. *Sci. Total Environ.* **2019**, *683*, 360–370. [CrossRef]
20. Lin, M.; Horowitz, L.W.; Oltmans, S.J.; Fiore, A.M.; Fan, S. Tropospheric ozone trends at Mauna Loa Observatory tied to decadal climate variability. *Nat. Geosci.* **2014**, *7*, 136–143. [CrossRef]
21. Xu, J.; Jia, H.; Zhou, H.; Kang, Y.; Zhong, K. Influences of offshore background wind on the formation of sea-land breeze and the characteristics of pollutant diffusion. *Environ. Sci. Pollut. Res. Int.* **2021**, *28*, 68318–68329. [CrossRef]

22. Camps, J.; Massons, J.; Soler, M.R.; Nickerson, E.C. Pollutant transport in coastal areas with and without background wind. *Ann. Geophys.* **1997**, *15*, 476–486. [CrossRef]

23. Lin, S.-L.; Deng, Y.; Huang, C.-E.; Tien, K.-K.; Lee, Y.-Y. Atmospheric PM2.5 near an Urban-Industrial Complex during Air-pollution Episodes with Various Meteorological Conditions. *Aerosol Air Qual. Res.* **2022**, *22*, 220187. [CrossRef]

24. Tang, Y.; Yang, X.; Yang, J.; Cai, Z.; Han, S.; Shi, J.; Jiang, M.; Qiu, Y. Investigation of Coastal Atmospheric Boundary Layer and Particle by Unmanned Aerial Vehicle under Different Land-sea Temperature. *Aerosol Air Qual. Res.* **2022**, *22*, 220206. [CrossRef]

25. Darby, L.S. Cluster Analysis of Surface Winds in Houston, Texas, and the Impact of Wind Patterns on Ozone. *J. Appl. Meteorol.* **2005**, *44*, 1788–1806. [CrossRef]

26. Liu, Z.; Lu, X.; Feng, J.; Fan, Q.; Zhang, Y.; Yang, X. Influence of Ship Emissions on Urban Air Quality: A Comprehensive Study Using Highly Time-Resolved Online Measurements and Numerical Simulation in Shanghai. *Environ. Sci. Technol.* **2017**, *51*, 202–211. [CrossRef] [PubMed]

27. Shang, F.; Chen, D.; Guo, X.; Lang, J.; Zhou, Y.; Li, Y.; Fu, X. Impact of Sea Breeze Circulation on the Transport of Ship Emissions in Tangshan Port, China. *Atmosphere* **2019**, *10*, 723. [CrossRef]

28. Ma, Y.; Chen, D.; Fu, X.; Shang, F.; Guo, X.; Lang, J.; Zhou, Y. Impact of Sea Breeze on the Transport of Ship Emissions: A Comprehensive Study in the Bohai Rim Region, China. *Atmosphere* **2022**, *13*, 1094. [CrossRef]

29. Liu, H.; Chan, J.C.L. An investigation of air-pollutant patterns under sea–land breezes during a severe air-pollution episode in Hong Kong. *Atmos. Environ.* **2002**, *36*, 591–601. [CrossRef]

30. Zeng, L.P.; Lin, W.S.; Fan, Q.; Feng, Y.R. Simulation of Wind Circulation and Pollutant Diffusion Over the Pearl River Delta Region. *Environ. Model. Assess.* **2012**, *17*, 539–553. [CrossRef]

31. Li, H.; Huang, X.; Xu, Q.; Wang, S.; Guo, W.; Liu, Y.; Huang, Y.; Wang, J. A New Approach to Evaluate the Sustainability of Ecological and Economic Systems in Megacity Clusters: A Case Study of the Guangdong—Hong Kong—Macau Bay Area. *Sustainability* **2023**, *15*, 5881. [CrossRef]

32. World Shipping Council. Available online: https://www.worldshipping.org/top-50-ports (accessed on 9 April 2023).

33. Sun, K.; Liu, H.; Ding, A.; Wang, X. WRF-Chem Simulation of a Severe Haze Episode in the Yangtze River Delta, China. *Aerosol Air Qual. Res.* **2016**, *16*, 1268–1283. [CrossRef]

34. Mao, J.; Zhang, Y.; Yu, F.; Chen, J.; Sun, J.; Wang, S.; Zou, Z.; Zhou, J.; Yu, Q.; Ma, W.; et al. Simulating the impacts of ship emissions on coastal air quality: Importance of a high-resolution emission inventory relative to cruise- and land-based observations. *Sci. Total Environ.* **2020**, *728*, 138454. [CrossRef] [PubMed]

35. Garcia, J.A.; Vallar, E.; Galvez, M.C.; Bagtasa, G. Application of the WRF/Chem v.3.6.1 on the reanalysis of criteria pollutants over Metro Manila. *Sustain. Environ. Res.* **2019**, *29*, 38. [CrossRef]

36. Le, T.; Wang, Y.; Liu, L.; Yang, J.; Yung, Y.L.; Li, G.; Seinfeld, J.H. Unexpected air pollution with marked emission reductions during the COVID-19 outbreak in China. *Science* **2020**, *369*, 702–706. [CrossRef] [PubMed]

37. Yun, X.; Shen, G.; Shen, H.; Meng, W.; Chen, Y.; Xu, H.; Ren, Y.; Zhong, Q.; Du, W.; Ma, J.; et al. Residential solid fuel emissions contribute significantly to air pollution and associated health impacts in China. *Sci. Adv.* **2020**, *6*, eaba7621. [CrossRef] [PubMed]

38. Xing, L.; Fu, T.M.; Liu, T.Y.; Qin, Y.M.; Zhou, L.Y.; Chan, C.K.; Guo, H.; Yao, D.W.; Duan, K.Q. Estimating organic aerosol emissions from cooking in winter over the Pearl River Delta region, China. *Environ. Pollut.* **2022**, *292*, 118266. [CrossRef]

39. Wesely, M.L. Parameterization of surface resistances to gaseous dry deposition in regional-scale numerical models. *Atmos. Environ.* **1989**, *23*, 1293–1304. [CrossRef]

40. Tie, X. Effect of clouds on photolysis and oxidants in the troposphere. *J. Geophys. Res.* **2003**, *108*, D20. [CrossRef]

41. Ansari, T.U.; Ojha, N.; Chandrasekar, R.; Balaji, C.; Singh, N.; Gunthe, S.S. Competing impact of anthropogenic emissions and meteorology on the distribution of trace gases over Indian region. *J. Atmos. Chem.* **2016**, *73*, 363–380. [CrossRef]

42. Chen, D.; Zhang, Y.; Lang, J.; Ying, Z.; Li, Y.; Guo, X.; Wang, W.; Liu, B. Evaluation of different control measures in 2014 to mitigate the impact of ship emissions on air quality in the Pearl River Delta, China. *Atmos. Environ.* **2019**, *216*, 116911. [CrossRef]

43. Stockwell, W.R.; Middleton, P.; Chang, J.S.; Tang, X. The second generation regional acid deposition model chemical mechanism for regional air quality modeling. *J. Geophys. Res. Atmos.* **1990**, *95*, 16343–16367. [CrossRef]

44. Schell, B.; Ackermann, I.J.; Hass, H.; Binkowski, F.S.; Ebel, A. Modeling the formation of secondary organic aerosol within a comprehensive air quality model system. *J. Geophys. Res. Atmos.* **2001**, *106*, 28275–28293. [CrossRef]

45. Ackermann, I.J.; Hass, H.; Memmesheimer, M.; Ebel, A.; Binkowski, F.S.; Shankar, U. Modal aerosol dynamics model for Europe: Development and first applications. *Atmos. Environ.* **1998**, *32*, 2981–2999. [CrossRef]

46. Hong, S.Y.; Noh, Y.; Dudhia, J. A new vertical diffusion package with an explicit treatment of entrainment processes. *Mon. Weather. Rev.* **2006**, *134*, 2318–2341. [CrossRef]

47. Fels, S.B.; Schwarzkopf, M.D. An efficient, accurate algorithm for calculating CO_2 15 μm band cooling rates. *J. Geophys. Res. Ocean.* **1981**, *86*, 1205–1232. [CrossRef]

48. Chou, M.D. A solar radiation parameterization for atmospheric studies. *J. Nasa Tech. Memo* **1999**, *15*, 40.

49. Lin, Y.L. Bulk parameterization of the snow field in a cloud model. *J. Appl. Meteorol. Climatol.* **1983**, *22*, 1065–1092. [CrossRef]

50. Ek, M.B.; Mitchell, K.E.; Lin, Y.; Rogers, E.; Grunmann, P.; Koren, V.; Gayno, G.; Tarpley, J.D. Implementation of Noah land surface model advances in the National Centers for Environmental Prediction operational mesoscale Eta model. *J. Geophys. Res. Atmos.* **2003**, *108*, D22. [CrossRef]

51. NCEP. Available online: https://rda.ucar.edu/datasets/ds083.2/ (accessed on 11 February 2021).

52. Chen, D.; Wang, X.; Li, Y.; Lang, J.; Zhou, Y.; Guo, X.; Zhao, Y. High-spatiotemporal-resolution ship emission inventory of China based on AIS data in 2014. *Sci. Total Environ.* **2017**, *609*, 776–787. [CrossRef]

53. Multi-Resolution Emission Inventory for China. Available online: http://www.meicmodel.org/ (accessed on 2 March 2022).

54. Liu, F.; Zhang, Q.; Tong, D.; Zheng, B.; Li, M.; Huo, H.; He, K.B. High-resolution inventory of technologies, activities, and emissions of coal-fired power plants in China from 1990 to 2010. *Atmos. Chem. Phys.* **2015**, *15*, 13299–13317. [CrossRef]

55. Peng, L.; Zhang, Q.; Yao, Z.; Mauzerall, D.L.; Kang, S.; Du, Z.; Zheng, Y.; Xue, T.; He, K. Underreported coal in statistics: A survey-based solid fuel consumption and emission inventory for the rural residential sector in China. *Appl. Energy* **2019**, *235*, 1169–1182. [CrossRef]

56. Tong, D.; Zhang, Q.; Liu, F.; Geng, G.; Zheng, Y.; Xue, T.; Hong, C.; Wu, R.; Qin, Y.; Zhao, H.; et al. Current Emissions and Future Mitigation Pathways of Coal-Fired Power Plants in China from 2010 to 2030. *Environ. Sci. Technol.* **2018**, *52*, 12905–12914. [CrossRef]

57. Zhang, Q.; Streets, D.G.; Carmichael, G.R.; He, K.B.; Huo, H.; Kannari, A.; Klimont, Z.; Park, I.S.; Reddy, S.; Fu, J.S.; et al. Asian emissions in 2006 for the NASA INTEX-B mission. *Atmos. Chem. Phys.* **2009**, *9*, 5131–5153. [CrossRef]

58. Zheng, B.; Huo, H.; Zhang, Q.; Yao, Z.L.; Wang, X.T.; Yang, X.F.; Liu, H.; He, K.B. High-resolution mapping of vehicle emissions in China in 2008. *Atmos. Chem. Phys.* **2014**, *14*, 9787–9805. [CrossRef]

59. Zheng, B.; Tong, D.; Li, M.; Liu, F.; Hong, C.; Geng, G.; Li, H.; Li, X.; Peng, L.; Qi, J.; et al. Trends in China's anthropogenic emissions since 2010 as the consequence of clean air actions. *Atmos. Chem. Phys.* **2018**, *18*, 14095–14111. [CrossRef]

60. Zhou, Y.; Xing, X.F.; Lang, J.L.; Chen, D.S.; Cheng, S.Y.; Wei, L.; Wei, X.; Liu, C. A comprehensive biomass burning emission inventory with high spatial and temporal resolution in China. *Atmos. Chem. Phys.* **2017**, *17*, 2839–2864. [CrossRef]

61. NCAR. Available online: https://www2.acom.ucar.edu/wrf-chem/wrf-chem-tools-community#download/ (accessed on 18 May 2021).

62. NCEI. Available online: https://gis.ncdc.noaa.gov/maps/ncei/cdo/hourly/ (accessed on 5 May 2022).

63. Kwok, R.H.F.; Fung, J.C.H.; Lau, A.K.H.; Fu, J.S. Numerical study on seasonal variations of gaseous pollutants and particulate matters in Hong Kong and Pearl River Delta Region. *J. Geophys. Res.* **2010**, *115*, D16. [CrossRef]

64. Zhang, Y.; Liu, P.; Pun, B.; Seigneur, C. A comprehensive performance evaluation of MM5-CMAQ for the Summer 1999 Southern Oxidants Study episode—Part I: Evaluation protocols, databases, and meteorological predictions. *Atmos. Environ.* **2006**, *40*, 4825–4838. [CrossRef]

65. U.S. EPA. *Guidance on the Use of Models and Other Analyses for Demonstrating Attainment of Air Quality Goals For Ozone, PM2.5, and Regional Haze*; US Environmental Protection Agency: Research Triangle Park, NC, USA, 2007. Available online: https://www.epa.gov/sites/default/files/2020-10/documents/final-03-pm-rh-guidance.pdf (accessed on 5 May 2023).

66. Boylan, J.W.; Russell, A.G. PM and light extinction model performance metrics, goals, and criteria for three-dimensional air quality models. *Atmos. Environ.* **2006**, *40*, 4946–4959. [CrossRef]

67. SethuRaman, S.; Raynor, G.S. Comparison of Mean Wind Speeds and Turbulence at a Coastal Site and an Offshore Location. *J. Appl. Meteorol.* **1980**, *19*, 15–21. [CrossRef]

68. Zhang, Y.-L.; Cao, F. Fine particulate matter ($PM_{2.5}$) in China at a city level. *Sci. Rep.* **2015**, *5*, 14884. [CrossRef]

69. Lu, X.; Chen, Y.; Huang, Y.; Lin, C.; Li, Z.; Fung, J.C.H.; Lau, A.K.H. Differences in concentration and source apportionment of PM(2.5) between 2006 and 2015 over the PRD region in southern China. *Sci. Total Environ.* **2019**, *673*, 708–718. [CrossRef]

70. Sillman, S. The relation between ozone, NOx and hydrocarbons in urban and polluted rural environments. *Atmos. Environ.* **1999**, *33*, 1821–1845. [CrossRef]

71. Jenkin, M.E.; Clemitshaw, K.C. Ozone and other secondary photochemical pollutants: Chemical processes governing their formation in the planetary boundary layer. *Atmos. Environ.* **2000**, *34*, 2499–2527. [CrossRef]

72. Yau, P.S.; Lee, S.C.; Cheng, Y.; Huang, Y.; Lai, S.C.; Xu, X.H. Contribution of ship emissions to the fine particulate in the community near an international port in Hong Kong. *Atmos. Res.* **2013**, *124*, 61–72. [CrossRef]

73. Wang, N.; Lyu, X.; Deng, X.; Huang, X.; Jiang, F.; Ding, A. Aggravating O_3 pollution due to NOx emission control in eastern China. *Sci. Total Environ.* **2019**, *677*, 732–744. [CrossRef] [PubMed]

74. Chen, X.; Situ, S.; Zhang, Q.; Wang, X.; Sha, C.; Zhouc, L.; Wu, L.; Wu, L.; Ye, L.; Li, C. The synergetic control of NO_2 and O_3 concentrations in a manufacturing city of southern China. *Atmos. Environ.* **2019**, *201*, 402–416. [CrossRef]

75. Du, Y.; Zhao, K.; Yuan, Z.; Luo, H.; Ma, W.; Liu, X.; Wang, L.; Liao, C.; Zhang, Y. Identification of close relationship between large-scale circulation patterns and ozone-precursor sensitivity in the Pearl River Delta, China. *J. Environ. Manag.* **2022**, *312*, 114915. [CrossRef]

76. Gong, X.; Hong, S.; Jaffe, D.A. Ozone in China: Spatial Distribution and Leading Meteorological Factors Controlling O_3 in 16 Chinese Cities. *Aerosol Air Qual. Res.* **2018**, *18*, 2287–2300. [CrossRef]

77. Wu, Y.K.; Chen, W.H.; Yan, F.H.; Mao, J.Y.; Yuan, B.; Wang, W.W.; Wang, X.M. Nonlinear Response Relationship Between Ozone and Precursor Emissions in the Pearl River Delta Region Under Different Transmission Channels. *Environ. Sci.* **2022**, *43*, 160–169. (In Chinese) [CrossRef]

78. Itahashi, S.; Uno, I.; Kim, S. Seasonal source contributions of tropospheric ozone over East Asia based on CMAQ–HDDM. *Atmos. Environ.* **2013**, *70*, 204–217. [CrossRef]

79. Liu, X.-H.; Zhang, Y.; Xing, J.; Zhang, Q.; Wang, K.; Streets, D.G.; Jang, C.; Wang, W.-X.; Hao, J.-M. Understanding of regional air pollution over China using CMAQ, part II. Process analysis and sensitivity of ozone and particulate matter to precursor emissions. *Atmos. Environ.* **2010**, *44*, 3719–3727. [CrossRef]

80. Chen, Y.; Yan, H.; Yao, Y.; Zeng, C.; Gao, P.; Zhuang, L.; Fan, L.; Ye, D. Relationships of ozone formation sensitivity with precursors emissions, meteorology and land use types, in Guangdong-Hong Kong-Macao Greater Bay Area, China. *J. Environ. Sci.* **2020**, *94*, 1–13. [CrossRef] [PubMed]

81. Chang, L.S.; Lee, G.; Im, H.; Kim, D.; Park, S.M.; Choi, W.J.; Lee, Y.; Lee, D.W.; Kim, D.G.; Lee, D.; et al. Quantifying the Impact of Synoptic Weather Systems on High PM2.5 Episodes in the Seoul Metropolitan Area, Korea. *J. Geophys. Res. Atmos.* **2021**, *126*, e2020JD034085. [CrossRef]

82. Santos, M.D.; Dawidowski, L.; Smichowski, P.; Ulke, A.G.; Gómez, D. Factors controlling sea salt abundances in the urban atmosphere of a coastal South American megacity. *Atmos. Environ.* **2012**, *59*, 483–491. [CrossRef]

83. Yu, J.Z.; Tung, J.W.T.; Wu, A.W.M.; Lau, A.K.H.; Louie, P.K.K.; Fung, J.C.H. Abundance and seasonal characteristics of elemental and organic carbon in Hong Kong PM10. *Atmos. Environ.* **2004**, *38*, 1511–1521. [CrossRef]

84. Wang, X.; Zhang, Y.; Hu, Y.; Zhou, W.; Zeng, L.; Hu, M.; Cohan, D.S.; Russell, A.G. Decoupled direct sensitivity analysis of regional ozone pollution over the Pearl River Delta during the PRIDE-PRD2004 campaign. *Atmos. Environ.* **2011**, *45*, 4941–4949. [CrossRef]

85. Safieddine, S.; Boynard, A.; Hao, N.; Huang, F.; Wang, L.; Ji, D.; Barret, B.; Ghude, S.D.; Coheur, P.F.; Hurtmans, D.; et al. Tropospheric ozone variability during the East Asian summer monsoon as observed by satellite (IASI), aircraft (MOZAIC) and ground stations. *Atmos. Chem. Phys.* **2016**, *16*, 10489–10500. [CrossRef]

86. Zhao, C.; Wang, Y.; Yang, Q.; Fu, R.; Cunnold, D.; Choi, Y. Impact of East Asian summer monsoon on the air quality over China: View from space. *J. Geophys. Res.* **2010**, *115*, D9. [CrossRef]